

Constraining $f(R)$ gravity with PLANCK data on galaxy cluster profiles

I. De Martino^{1,4*}, M. De Laurentis^{2,3,4}, F. Atrio-Barandela¹, S. Capozziello^{3,4}

¹ *Física Teórica, Universidad de Salamanca, 37008 Salamanca, Spain; email: ivan.demartino@usal.es; atrio@usal.es*

² *Department of Theoretical Physics, Tomsk State Pedagogical University (TSPU), pr. Komsomolsky, 75, Tomsk, 634041, Russia*

³ *Dipartimento di Fisica, Università di Napoli "Federico II"*

⁴ *INFN sez. di Napoli Compl. Univ. di Monte S. Angelo, Edificio G, Via Cinthia, I-80126 - Napoli, Italy*

Accepted xxxx Yyyber zz. Received xxxx Yyyember zz; in original form xxxx Yyyber zz

ABSTRACT

Models of $f(R)$ gravity that introduce corrections to the Newtonian potential in the weak field limit are tested at the scale of galaxy clusters. These models can explain the dynamics of spiral and elliptical galaxies without resorting to dark matter. We compute the pressure profiles of 579 galaxy clusters assuming that the gas is in hydrostatic equilibrium within the potential well of the modified gravitational field. The predicted profiles are compared with the average profile obtained by stacking the data of our cluster sample in the Planck foreground clean map SMICA. We find that the resulting profiles of these systems fit the data without requiring a dominant dark matter component, with model parameters similar to those required to explain the dynamics of galaxies. Our results do not rule out that clusters are dynamically dominated by Dark Matter but support the idea that Extended Theories of Gravity could provide an explanation to the dynamics of self-gravitating systems and to the present period of accelerated expansion, alternative to the concordance cosmological model.

1 INTRODUCTION

Measurements based on Supernovae Type Ia (SNeIa) have indicated that the Universe has entered a period of accelerated expansion (Riess et al. 2004; Astier et al. 2006; Clocchiati 2006). Data on Cosmic Microwave Background (CMB) temperature anisotropies measured by the Wilkinson Microwave Anisotropy Probe (WMAP) (Hinshaw et al. 2013) and the Planck satellite (Planck Results XV 2013; Planck Results XVI 2013; Planck Results XX 2013; Planck Results XXI 2013), on Baryon Acoustic Oscillations (BAO) (Blake et al. 2011) and other observables, together with SNeIa data, favor the concordance Λ CDM model. In this model, the energy component that drives the current period of accelerated expansion is a cosmological constant Λ . The associated energy density is $\Omega_\Lambda \simeq 0.7$, in units of the critical density. The second most important component is Dark Matter (DM), a matter component required to explain the formation of galaxies and the emergence of Large Scale Structure, with $\Omega_{DM} \simeq 0.26$. More general models assume that the acceleration is due to an evolving form of Dark Energy (DE) characterized by an equation of state parameter $w \leq -1/3$. For these models, cosmological observations indicate that $w = -1.13_{-0.10}^{+0.13}$ (Planck Results XVI 2013), fully compatible with a cosmological constant ($w = -1$).

As an alternative, models involving extensions of General Relativity (GR) have also been widely considered (for comprehensive reviews see Carroll et al. (2004), Sotiriou & Faroni (2010), De Felice & Tsujikawa (2013), Nojiri & Odintsov (2011), Nojiri & Odintsov (2011) and

Capozziello & De Laurentis (2011)). In this approach, the Hilbert-Einstein action changes from being linear in the Ricci curvature scalar, R , to a more general function. The simplest extensions are $f(R)$ models, where the Lagrangian is a function (possibly analytic) of the Ricci scalar. In these models, the higher order gravity terms introduced in the action are responsible for the present period of accelerated expansion. In some Extended Theories of Gravity (ETG), the Newtonian limit is also modified and models have been constructed where the dynamics of galaxies can be explained without requiring a DM component. For instance, analytic $f(R)$ models give rise to Yukawa-like correction to the gravitational potential (Capozziello & De Laurentis 2011, 2012) that do not require DM to explain the flat rotation curves of spiral galaxies (Cardone & Capozziello 2011) or the velocity dispersion of ellipticals (Napolitano et al. 2012). The constraints derived from planetary dynamics are weak since the Yukawa correction is negligible at those scales (Capozziello & Troisi 2005; Allemandi et al. 2005; Berry & Gair 2011). ETG also modify the hydrostatic equilibrium of stars: Capozziello et al. (2011), Farinelli et al. (2013) have compared the Lane-Emden solution of polytropic gases in both $f(R)$ and general relativity and found them to be compatible while Capozziello et al. (2012) analyzed Jeans instabilities in self-gravitating systems and studied star formation in $f(R)$ gravity.

Since the exact functional form of the Lagrangian is unknown, theoretical considerations need to be complemented with observations. Thus, it is important to test potential

models using all available data. At present, clusters of galaxies are the largest virialized objects in the Universe and offer the opportunity to test these alternative theories of gravity on scales larger than galaxy scales. Using the mass profiles of clusters of galaxies, Capozziello, De Filippis & Salzano (2009) showed that ETG provide a fit to the distribution of baryonic matter (stars+gas) derived from X-ray observations in 12 clusters without requiring DM. Nevertheless, in conventional cosmological models, the non-linear evolution and virialization of self-gravitating objects is studied using numerical simulations. $f(R)$ models have a much larger number of degrees of freedom and the study of galaxy and cluster formation requires more complex simulations, specific for each particular Lagrangian. A first attempt to constrain ETG using cluster abundances in numerical simulations has been carried out by Ferraro, Schimdt & Hu (2011) and Schimdt, Vikhlinin & Hu (2009). Other numerical constraints on $f(R)$ models can be found in Song, Hu & Sawicki (2007), Sawicki & Hu (2007), Hu & Sawicki (2007a,b) and Lima & Liddle (2013). More promising is the study of temperature fluctuations on the CMB. Galaxy clusters are reservoirs of hot gas that induces anisotropies by means of the Sunyaev-Zeldovich (SZ) effect (Sunyaev & Zeldovich 1972, 1980). Pressure profiles of galaxies can be computed in ETG assuming that the gas is in hydrostatic equilibrium within the potential well of clusters. This is in agreement with the results of numerical simulations based on the concordance cosmology that showed that gas is in hydrostatic equilibrium in the intermediate regions of clusters, while in the cluster cores, the physics of baryons is more complex and in the outer regions it is dominated by non-equilibrium processes (Kravtsov & Borgani 2012). Recently, hydro-numerical simulations are being carried out to study the properties of galaxy clusters and groups in ETG. Arnold, Puchwein & Springel (2013) showed that the intra-cluster medium temperature increases in $f(R)$ gravity in low mass halos but the difference disappears in massive objects. Based on these results we will assume that the physics of the gas will be weakly dependent on the underline theory of gravity.

The SZ anisotropies generated by individual clusters and by the unresolved cluster population have been measured by the Atacama Cosmology Telescope (ACT) (Hand et al. 2011; Hasselfield et al. 2013; Menanteau et al. 2013; Sehgal et al. 2011), the South Pole Telescope (SPT) (Benson et al. 2013; Staniszewsk et al. 2009; Williamson et al. 2011; Vanderlinde et al. 2010) and the Planck satellite (Planck Intermediate Results V 2013; Planck Intermediate Results X 2013; Planck Results XX 2013; Planck Results XXIX 2013). Gas profiles based on the Navarro-Frenk-White (hereafter NFW, Navarro et al. (1997)) profile, derived from numerical simulations, have been found to be in agreement with TSZ (Atrio-Barandela et al. 2008) and X-ray observations (Arnaud et al. 2010). Nevertheless, the contribution of the unresolved cluster population in WMAP 7yr data has been found to be smaller than expected based on theoretical and numerical modeling of clusters (Komatsu et al. 2011). For the Coma cluster, the analysis of Planck data (Planck Intermediate Results V 2013; Planck Intermediate Results X 2013) finds a normalization of $\sim 10 - 15\%$ lower compared with the parameters

derived from XMM observations. These discrepancies can be related to the existence of complex structures and sub-structures in clusters of galaxies as well as to the limitations of the theoretical modeling (Fusco-Femiano et al. 2013), that is the approach we are going to consider here.

In this article, we will compare the pressure profiles of clusters of galaxies in $f(R)$ models with Planck data. To construct the pressure profiles, we will assume that the gas is in hydrostatic equilibrium within the potential well generated by the cluster. At this level, our assumption can not be applied to models not in equilibrium like the Bullet cluster (Clowe et al. 2006). We will restrict our analysis to $f(R)$ models of gravity that introduce Yukawa corrections to the Newtonian potential in order to test if the dynamics of clusters of galaxies can be also described without a dominant dark matter component. The paper is organized as follows: in Sec. 2, we consider the weak field limit of $f(R)$ gravity deriving the gravitational potential for self-gravitating objects; in Sec. 3, we present the pressure profiles based on the NFW profile and X-ray data most commonly used and we compute the pressure profile for $f(R)$ models; in Sec. 4 we describe the data used in our analysis; in Sec. 5, we discuss our results and, finally, in Sec. 6 we present our main conclusions.

2 YUKAWA CORRECTIONS TO THE NEWTONIAN POTENTIAL IN $F(R)$ -GRAVITY

In $f(R)$ ETG, field equations are derived from the action

$$A = \frac{c^4}{16\pi G} \int d^4x \sqrt{-g} f(R) + \mathcal{L}_m, \quad (1)$$

yielding

$$f'(R)R_{\mu\nu} - \frac{f(R)}{2} g_{\mu\nu} - f'(R)_{;\mu\nu} + g_{\mu\nu} \square_g f'(R) = 8\pi G T_{\mu\nu},$$

where $f'(R) = df(R)/dR$ is the first derivative with respect to the Ricci scalar, $\square_g = ;\sigma;\sigma$ is the d'Alembertian with covariant derivatives, $T_{\mu\nu} = -2(-g)^{-1/2} \delta(\sqrt{-g}\mathcal{L}_m)/\delta g^{\mu\nu}$ is the matter energy-momentum tensor, T its trace, g the determinant of the metric tensor $g_{\mu\nu}$. Greek indices run from 0 to 3.

We search for spherically symmetric solutions of the form

$$ds^2 = g_{tt}c^2 dt^2 - g_{rr}dr^2 - r^2 d\Omega, \quad (2)$$

where $d\Omega$ is the solid angle. Let us restrict our study to those $f(R)$ -Lagrangians that can be expanded in Taylor series around a fixed point R_0

$$f(R) = \sum_n \frac{f^n(R_0)}{n!} (R - R_0)^n \simeq f_0 + f'_0 R + \frac{f''_0}{2} R^2 + \dots \quad (3)$$

The fixed point represents the Ricci-scalar in GR for the same mass distribution. In this case f_0 is a cosmological constant and $f'_0 = 1$. Then, the field Eqs. (2) can be solved at different orders in terms of the Taylor expansion. In the Newtonian limit the first correction is of order c^2 . The metric

tensor can be written as

$$g_{tt} \simeq 1 + 2\Phi_{grav}(r), \quad (4)$$

$$g_{rr} \simeq -(1 + \Phi_N(r)), \quad (5)$$

$$g_{\theta\theta} \simeq -r^2, \quad (6)$$

$$g_{\phi\phi} \simeq -r^2 \sin^2 \theta, \quad (7)$$

where

$$\Phi_N(r) = -\frac{GM(r)}{r}, \quad \Phi_{grav}(r) = \frac{\Phi_N(r)}{(1+\delta)} \left(1 + \delta e^{-\frac{r}{L}}\right), \quad (8)$$

Analytic $f(R)$ models that modify the Newtonian limit can be seen as alternative to Dark Matter. The Yukawa correction to the gravitational field allows us to study the dynamics of galaxies without requiring dark matter. The parameters (δ, L) are related to the coefficients in the Taylor expansion as: $f'_0 = 1 + \delta$ and $L = [-f'_0/(6f''_0)]^{1/2}$, where δ represents the deviation from GR at zero order and L the scale length of the self-gravitating object (Capozziello & De Laurentis 2011, 2012). In the limit $\delta = 0$, we recover the Newtonian limit of GR, irrespective of the scale parameter L . In ETG, L depends on the scale of the system considered; it assumes different values for the various self-gravitating systems like galaxies or cluster of galaxies while its effects are totally negligible at Solar System scales where GR, i.e. the Newtonian limit, is totally restored (Capozziello & De Laurentis 2012).

The physical meaning of the characteristic length L deserves further discussion. As pointed out in Capozziello & De Laurentis (2011), L can be seen as an extra *gravitational radius* similar to the Schwarzschild radius. Compared with GR, that is a second order theory, $f(R)$ gravity is fourth-order and contains a larger number of degrees of freedom that, in the weak field limit, give rise to a new characteristic scale length. The paradigm can be extended to $(2k+2)$ -order theories of gravity so any further two derivation orders imply a new characteristic length in the Newtonian limit (see Quandt & Schmidt (1991) for details), resulting in some important implications for the theory. First gravity is no longer a scale invariant interaction but depends on the size of the self-gravitating systems. In other words, gravitational corrections emerge depending on scales. Second, the Gauss theorem does not hold at finite scales but only asymptotically. This is not a problem since Bianchi identities hold for $f(R)$ as for any ETG theory and conservation laws are fulfilled like in GR. Third, GR is totally restored at Solar System scales so $f(R)$ theory agrees with standard classical tests (Capozziello & Tsujikawa 2008). Finally, the approach allows to represent DM effects only by gravity without requiring new ingredients at the fundamental level. This fact could be considered as an astrophysical testbed for relativistic theories of gravity since the additional gravitational length L introduced in this model could be accurately matched with observational data as we are going to show below.

3 CLUSTER PRESSURE PROFILES IN $F(R)$ GRAVITY

Model	c_{500}	α_a	β_a	γ_a	P_0
Arnaud	1.177	1.051	5.4905	0.3081	$8.403h_{70}^{3/2}$
Planck	1.81	1.33	4.13	0.31	6.41
Sayers	1.18	0.86	3.67	0.67	4.29
β	β	$n_{c,0}/m^{-3}$	r_c/Mpc	T_e/keV	
	2/3	3860.	0.25	6.48	
$f(R)$	δ	L/Mpc	γ		
	-0.98	0.1	1.2		

Table 1. Parameters of the Generalized NFW, β and $f(R)$ models represented in Fig. 1; the Generalized NFW pressure profile data is from Arnaud et al. (2010), Planck Intermediate Results V (2013) and Sayers et al. (2013), the β -model data corresponds to the Coma cluster and the $f(R)$ profile data is the best fit model to Planck data (see Sec. 5).

When CMB photons cross the potential wells of clusters of galaxies, they are scattered off by the electrons of the Intra-Cluster medium, inducing secondary temperature anisotropies on the CMB of two different type by means of the SZ effect: a thermal contribution due to the motion of the electrons within the cluster potential well and kinematic one (KSZ) due to the motion of the cluster as a whole. The TSZ is the only SZ anisotropy that has been measured for individual clusters and is given by (Sunyaev & Zeldovich 1972)

$$\frac{\Delta T}{T_0} = g(\nu) \frac{k_B \sigma_T}{m_e c^2} \int n_e T_e dl, \quad (9)$$

where T_e is the electron temperature, n_e the electron density and the integration is carried out along the line of sight l . In Eq. (9) k_B is the Boltzmann constant, $m_e c^2$ the electron annihilation temperature, c the speed of light, ν the frequency of observation, σ_T Thomson cross section and T_0 the mean temperature of the CMB. Finally, $g(\nu) = x \coth(x/2) - 4$ is the frequency dependence of the TSZ effect, with $x = h\nu/KT_0$.

To compute the TSZ anisotropy we need to specify the pressure profile $n_e T_e$ of clusters. Using X-ray data and numerical simulations, several cluster profiles have appeared in the literature:

- The X-ray emitting region of clusters of galaxies is well fit by the isothermal β -model profiles (Cavaliere & Fusco-Femiano 1976, 1978). In this model, the electron density is given by: $n_e(r) = n_{e,0} [1 + (r/r_c)^2]^{-3\beta/2}$, where the core radius r_c , the central electron density $n_{e,0}$, the electron temperature and the slope β need to be determined from observations. From the X-ray surface brightness of clusters, $\beta = 0.6 - 0.8$ (Jones & Forman 1984). In Table 1 we give the value of the β model parameters of the Coma cluster.

- Outside the central cluster regions, the β model overpredicts the TSZ contribution (Atrio-Barandela et al. 2008). If the electrons are in hydrostatic equilibrium within the potential well of dark matter halos, the pressure profile is well describe by a Komatsu-Seljak model (Komatsu & Seljak 2002; Atrio-Barandela et al. 2008). More recently, Arnaud et al. (2010) proposed a phenomeno-

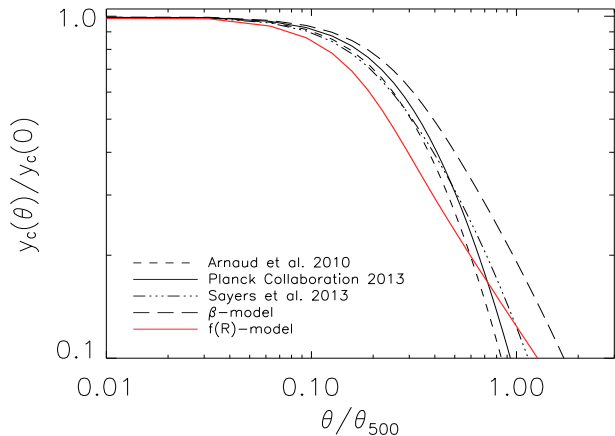


Figure 1. Pressure profiles integrated along the line of sight for the Coma cluster. We represent three GFW profiles (dashed, solid and dash-dotted lines), one $\beta = 2/3$ model (long dashed line) and a $f(R)$ model (red solid line). The model parameters are given in Table 1. The angular diameter distance is that of the Coma cluster ($z = 0.023$).

logical parametrization of the electron pressure profile based on generalized Navarro-Frenk-White (GFW) profiles derived from the numerical simulations of Nagai et al. (2007). This profile has the following functional form

$$p(x) \equiv \frac{P_0}{(c_{500}x)^{\gamma_a} [1 + (c_{500}x)^{\alpha_a}]^{(\beta_a - \gamma_a)/\alpha_a}}, \quad (10)$$

In this expression x is the radial distance in units of r_{500} , the radius where the average density is 500 times the critical density, and c_{500} is the concentration parameter at r_{500} . Different groups have fit the model parameters $[c_{500}, \alpha_a, \beta_a, \gamma_a, P_0]$ to X-ray or CMB data; their best fit values are given in Table 1.

GFW models fit the DM distribution in numerical simulations that use newtonian gravity and therefore can not be used to describe the dynamics in the ETG we are considering. Instead, baryons reside in the potential well of clusters. The Yukawa correction to the Newtonian potential of eq. (8) modifies the gravitational structure of clusters and there is not longer any need to introduce dark matter to explain their dynamics. In this limit, to compute the pressure profile $n_e T_e$ of Eq. (9) we assume that the gas is in hydrostatic equilibrium within the (modified) potential well of the cluster

$$\frac{dP(r)}{dr} = -\rho(r) \frac{d\Phi_{grav}(r)}{dr}, \quad (11)$$

and to describe the physical state of the gas we further assume that it follows a polytropic equation of state

$$P(r) \propto \rho^\gamma(r). \quad (12)$$

Eqs. (11) and (12) together with mass conservation

$$\frac{dM(r)}{dr} = 4\pi\rho(r), \quad (13)$$

and the cluster gravitational potential given by eq. (8) form a close system of equations that can be solved numerically to obtain the pressure profiles of any given cluster as a function of two gravitational parameter (δ, L) and the polytropic index γ . For illustration, in Fig. 1 we plot the different profiles integrated along the line of sight with the parameters

given in Table 1. We particularize the models for the Coma cluster. For convenience, all distances are written in units of r_{500} and the angular scale is $\theta_{500} = r_{500}/d_A^{Coma}$ where d_A^{Coma} is the angular diameter distance of Coma. Dashed, solid and dash-dotted lines correspond to GFW profiles with the Arnaud et al. (2010), Planck Intermediate Results V (2013) and Sayers et al. (2013) parameters, respectively. The long-dashed line corresponds to the β model and the red solid line to the $f(R)$ model.

4 DATA.

To constrain the ETG model described in Sec. 2, we will use the pressure profiles of clusters of galaxies given in Sec. 3. To that purpose we shall use Planck data and a proprietary cluster catalog.

4.1 The Cluster Catalog

Our cluster catalogue contains 579 clusters selected from ROSAT All Sky-Survey (RASS). Those clusters are outside the minimal Planck mask that removes a $\sim 20\%$ of the sky in the Plane of the Galaxy. Clusters are drawn from the three flux limited cluster samples: the extended Brightest Cluster Sample (eBCS, (Ebeling et al. 1998, 2000)), the ROSAT-ESO Flux Limited X-ray catalog (REFLEX, (Böhringer et al. 2004)), and the Clusters in the Zone of Avoidance (CIZA, (Ebeling et al. 2002; Kocevski et al. 2007)). For each cluster, the catalog lists position, flux, and luminosity measured directly from RASS data and spectroscopically measured redshifts. The X-ray electron temperature is derived from the $L_X - T_X$ relation of White et al. (1997). For each cluster, the spatial profile of the X-ray emitting gas is fit to a β -model convolved with the RASS point-spread function to the RASS data. Due to the poor sampling of the surface brightness profile for all but the most nearby clusters, β is fixed to the canonical value of $\beta = 2/3$ (Jones & Forman 1984) but the core radii r_c and central electron densities $n_{e,0}$ are derived from the data. Thus, our catalog provides enough information to compute the Comptonization parameter of the X-ray emitting region of all the clusters in our sample. In Atrio-Barandela et al. (2008), it was found that the predicted values and those measured in WMAP 3yr data were in agreement with the β model for the inner part of the clusters, being the discrepancy between the TSZ prediction and observation below 10%.

4.2 Cosmic Microwave Background data.

The release of WMAP 9yr data (Bennet et al. 2013) at the end of 2012 was followed by the first data release of the Planck satellite in April 2013. Nine maps spanning a frequency range from 32 to 845GHz have been made publicly available by the Planck Collaboration¹. While the WMAP team provided foreground clean maps of all Differencing Assemblies (DA), the Planck Collaboration did not validate foreground clean maps at all frequencies. Instead, they used component separation methods to construct a map of CMB

¹ <http://irsa.ipac.caltech.edu/Missions/planck.html>

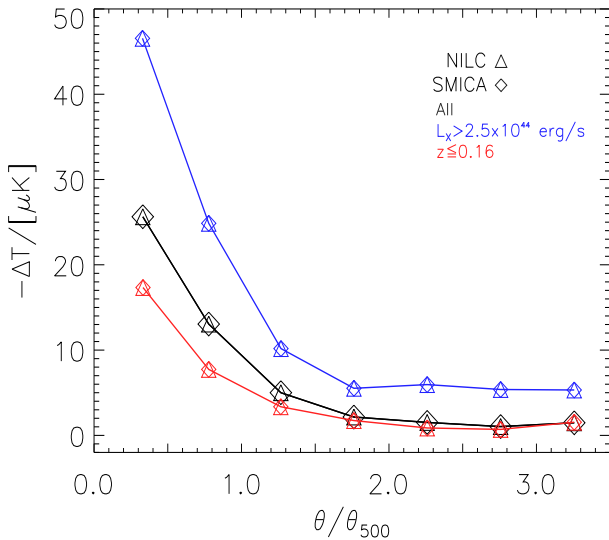


Figure 2. Average temperature anisotropy in the SMICA (diamonds) and NILC (triangles) maps at the position of two cluster subset selected according to luminosity and redshift (blue and red lines) and of our full sample (solid black line).

temperature anisotropies combining the data at all frequencies (Planck Results XII 2013). The SMICA map was produced by combining all nine Planck frequency maps, previously upgraded to the same resolution of $5'$, in spherical harmonic space using different weights at different multipoles. The NILC map was constructed in needlet space given different weights to the multipoles and to the spatial positions of the data in the sky. These two maps were constructed using different algorithms and, therefore, it is likely that they will differ in amplitude, distribution and spatial properties of the foreground residuals (Planck Results XIII 2013). We will perform our analysis in both foreground clean maps, both with Healpix resolution $N_{side} = 2048$ (Gorski et al. 2005), to test for systematics.

To compute the TSZ profile of the clusters in our sample, we average the temperature anisotropy at the cluster positions. At the cluster center the average is over a disc of radius $\theta_{500}/2$ where θ_{500} is the angular scale subtended by the r_{500} radius of the cluster. Outside the inner disc, we take the average on rings of width $\theta_{500}/2$. The measured value is the averaged over all clusters in our sample. The angular position θ we associate to each data point is the mean of the angular distance to the center of the cluster of every pixel in a disc or ring. The root mean square dispersion around the mean is about $0.1\theta_{500}$ for the central disc that contains the smallest number of pixels and is $0.05\theta_{500}$ or smaller for the rings. In Fig. 2, we present the results for the SMICA (diamonds) and NILC (triangles) maps. We compare the results on both maps for the full sample (solid black line) and for two cluster subsets, selected according to luminosity (blue) and redshift (red). The results of both maps differ by less than 1% in the three samples proving that the differences in the component separation method do not distort the TSZ anisotropy associated with clusters. The agreement between the TSZ profiles measured in the SMICA and NILC maps demonstrates that systematic effects will not affect our final results.

To each data point we associate an error bar obtained by evaluating 1,000 times the average profiles at 579 random positions in the SMICA and NILC maps. To avoid overlapping real and simulated clusters, we excise a disc of $80'$ around each cluster in our sample. The errors on both maps are also indistinguishable. For comparison, we analyzed the W-band of WMAP 9yr data. The results were very similar to those of Planck except for larger error bars. As remarked in Planck Results XII (2013), at high latitudes, outside the Galactic Plane, the amplitude of the foregrounds residuals present on the SMICA map is a few μK , smaller than those on the NILC map. Therefore, since NILC or WMAP do not provide extra information and since they are more affected by noise or foregrounds than SMICA, we will restrict our analysis to the latter data.

4.3 The average SZ profile

To compare cluster profiles with observations, we measure the angle subtended by every cluster in units of θ_{500} . For each cluster, the radial scale r_{500} can be derived using the following scaling relation Böhringer et al. (2007)

$$r_{500} = \frac{0.753h^{-1} \text{ Mpc}}{h(z)} \times \left(\frac{L_X}{10^{44}h^{-2} \text{ erg s}^{-1}} \right)^{0.228}, \quad (14)$$

The radius r_{500} will allow us to test if the characteristic scale of our ETG, L , depends on the cluster properties or not. We checked that our results did not depend on the uncertainties of eq. (14) and we will not consider them any further. Similarly, we did not consider other scaling relations based on different data (Piffaretti et al. 2011; Planck Early Results X 2013). Eqs. (8), (11), (12) and (13) allow us to compute the pressure profile of all clusters in the data as a function of three parameters: (δ, L, γ) . These profiles are integrated along the line of sight to be compared with those measured in the SMICA map. As indicated in Sec. 2, L characterizes the dependence of $f(R)$ gravity on the size of the gravitating system. We consider two parameterizations of L to test if the theory depends on the properties of the clusters: (A) $L = \zeta r_{500}$ is different for each cluster but depends homogeneously on r_{500} for the whole sample and (B) where L is the same for all clusters. In Fig. 3 we plot the pressure profile integrated along of line of sight, convolved with a gaussian beam of $5'$ resolution, for different model parameters. Our models only predict the profile but not the central anisotropy. For this reason, we normalize all our theoretical profiles to unity. The data is equally normalized by dividing all the averages by the mean temperature on a disc of $0.1\theta_{500}$ radius. Error bars are computed in the same manner, renormalizing the disc and rings at random positions on the sky by the mean on the central disc of $0.1\theta_{500}$. In Figs. 3a-c L is different for each cluster (Model A) and in Figs. 3d-f L is the same for all clusters (Model B). To avoid overcrowding the plots, we fixed $\gamma = 1.2$. In each panel we show the variation of the pressure profile with L . Notice that in Model B, when $L \geq 20\text{Mpc}$, the variations on the profile are small. This is logical since L is the scale length of the Yukawa correction, that becomes negligible for large values of L . For illustrative purposes we overplot the SMICA data shown in Fig. 2, normalized to unity, with their corresponding error bars.

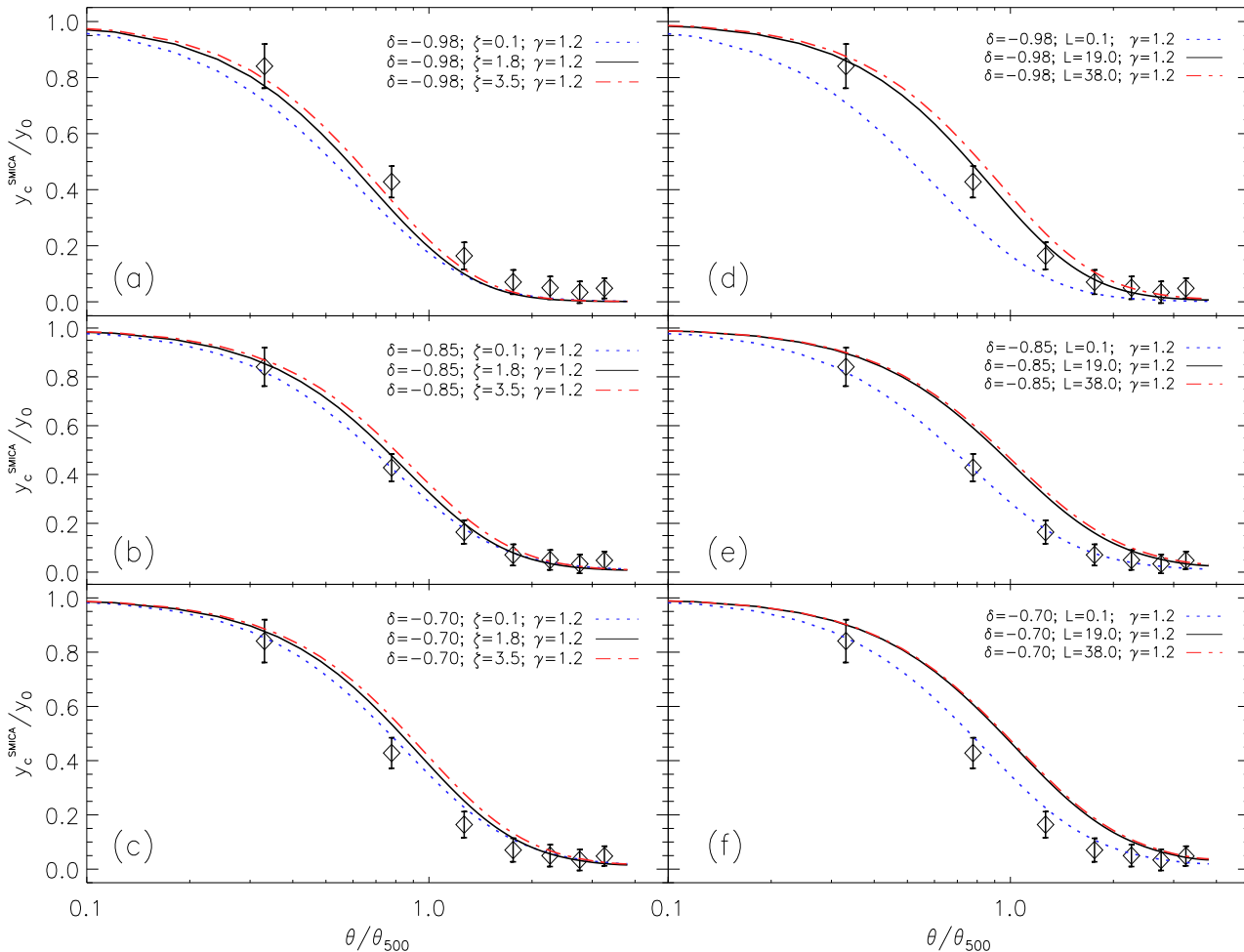


Figure 3. Pressure profiles of clusters in $f(R)$ gravity and SMICA data. Panels a-c correspond to the parametrization $L = \zeta r_{500}$ (Model A), while d-f correspond to the same scale L for all clusters (Model B).

5 RESULTS AND DISCUSSION

To determine the model parameters that best fit the SMICA data we generate pressure profiles for different values of the parameters (δ, L, γ) , integrated along the line of sight and convolved with a Gaussian beam with the same resolution of the SMICA map to compare them with the data. On physical grounds, we fix our parameter space to be $\delta = [-0.99, 1.0]$ since if $\delta < -1$ the potential is repulsive and diverges at $\delta = -1$. In the parametrization $L = \zeta r_{500}$ we take $\zeta = [0.1, 4]$. When L is the same for all clusters, we fix the interval to be $L = [0.1, 20]$ Mpc, from the scale of cluster core radius to the typical mean cluster separation scale. Finally, the polytropic equation of state parameter is set to vary within the range $\gamma = [1.0, 1.6]$, that corresponds to an isothermal and adiabatic monoatomic gas, respectively. We take 30 equally spaced steps in all intervals.

In Figs. 4 and 5, we compute the confidence contours for the different model parameters of Model A and Model B, respectively. The likelihood function $\log \mathcal{L} = -\chi^2/2$ is computed as

$$\chi^2(p) = \sum_{i,j=0}^N (y(p, x_i) - d(x_i)) C_{ij}^{-1} (y(p, x_j) - d(x_j)) \quad (15)$$

where $N = 7$ is the number of data points. The mean profile $y(p, x_i)$ of all the clusters in our sample depends on three

parameters: $p = (\delta, L, \gamma)$. In eq. (15), $d(x_i)$ is the SMICA average profile and $C_{i,j}$ is the correlation function between bins. To compute the correlation function we choose 579 random positions outside the locations of known clusters and compute the average temperature anisotropy on discs and rings of size θ_{500} , different for each of the random clusters. The process is repeated 1,000 times and $C_{i,j}$ is the average correlation between bins of any given cluster, averaged over all clusters and all simulations.

The value of the model A and B parameters that maximize the likelihood are given in Table 2. In Fig. 4 we plot the 68% and 95% confidence contours for pairs of parameters of Model A. Fig. 5 shows the same contours for the Model B. Since the models are very similar to each other, the likelihood function is flat close to the maximum. The 1σ contours are cut by our physical boundaries on δ and γ . Consequently, 2D contours of the marginalized likelihoods of pairs of parameters of these Figs are not closed, and only lower or upper limits to the parameters can be derived from their marginalized 1D likelihoods. At the 68% and 95% confidence levels those limits are $\delta < -0.46, -0.10$, $\zeta < 2.5, 3.7$ and $\gamma > 1.35, 1.12$ for the Model A parameters and $\delta < -0.43, -0.08$, $L < 12, 19$ Mpc and $\gamma > 1.45, 1.2$ for the Model B. In general, model parameters are weakly

constrained. In particular, the polytropic index constraints dominated by the physical boundary on this parameter. The characteristic scale length L is similar in both models, whether it scales with r_{500} or is identical for all clusters. In retrospect, this explains why the results of model A did not depend on the uncertainties in the scaling relation of r_{500} , given in eq. (14). But even if the parameters are weakly constrained, let us remark that in both models, A and B, the value $\delta = 0$ is excluded at more than a 95% confidence level. Since $\delta \simeq 0$ corresponds to the standard Newtonian potential without DM then the data does rule out that baryons alone are the dominant matter component in clusters.

The open contours in Figs. 4 and 5 reflect the physical limitations of our model. We can not extend our parameter space beyond $\delta = -1$. The limitation stems from the use of first order perturbations with respect to a background model. The contours show that at the 1σ level L is compatible with zero. Physically, at $L \simeq 0$ the gravitational field corresponds to the Newtonian potential generated by a mass $M' = M/(1+\delta)$. As $\delta+1 \simeq 0$ then $M' \gg M$ and the gravitational field is that of a system that contains a large fraction of DM distributed like the baryonic gas. Briefly, while our results show that cluster TSZ profiles in ETG are compatible with the data, they do not rule out that clusters could contain a significant fraction of DM. In summary, in order to fit the TSZ data, clusters are either dominated by DM or the Newtonian potential includes a Yukawa correction.

Comparison of Figs. 4 and 5 also shows that the data does not have enough statistical power to discriminate between Models A and B. Importantly, the results are consistent with those obtained by Sanders (1984) and Napolitano et al. (2012) using spiral and elliptical galaxies, respectively. In model A we find the same correlation between the gravity parameters L and δ that in the case of galaxies: to accommodate the data, larger values of L require lower values of δ , while the behavior is the opposite in Model B. This different scaling suggests that Model A is in better agreement with the dynamics of galaxies than Model B. Also, conceptually is the preferable model since L scales with the size of the self-gravitating system. The agreement of the central values of δ and L with those of galaxies, that correspond to a different linear scale, is very reassuring; the dynamics of galaxies and clusters can be equally described by ETG, without requiring DM. In other words, DM and alternative gravity models are equivalent descriptions that could be discriminated only by some signature at fundamental scales, i.e. the discovery of new particles non-interacting at electromagnetic level, or the clear evidence of some new gravitational mode not related to GR (Capozziello & De Laurentis (2011), Bogdanos et al. (2010)).

For comparison, we also compute the likelihood of each of the models given in Table 1 and their χ^2 per degree of freedom are given in Table 2. For the β model we generate the profile of each cluster using the data of our catalog. The β model does not produce a good fit to the data, in agreement with our previous results using WMAP data (Atrio-Barandela et al. 2008), since this model only fits the X-ray emitting regions of the inner parts of clusters. Comparing the three GFW parameters, the Arnaud et al. (2010) parameters, derived using the X-ray data of 33 clusters, performs better than either the

Planck Intermediate Results V (2013) or the Sayers et al. (2013) parameters, that were obtained from TSZ observations. These discrepancies are not relevant since we did not explore the parameter space to find the best fit values of GFW models to the SMICA data. Nevertheless, the fact that our $f(R)$ profiles fit significantly better than any other model is a clear indication that our assumption of a polytropic gas in hydrostatic equilibrium in the cluster potential well is supported by the data.

6 CONCLUSIONS

We have constructed cluster pressure profiles based on the Yukawa-like correction to the Newtonian potential obtained in the weak field approximation of $f(R)$ gravity. These models do not require large fractions of DM and they have been shown to describe well the dynamics of spiral and elliptical galaxies. By fitting the pressure profiles measured in the foreground clean SMICA map released by the Planck Collaboration, we have found that clusters can also be accurately described in these models. We have used a proprietary catalog of 579 clusters, and have determined the parameter space that best fits data. Our results are predicated on the baryonic gas being in hydrostatic equilibrium in the potential wells of clusters. This hypothesis can only be tested using hydrodynamical simulations and if the gas turn out not to be in equilibrium, our conclusion will be severely weakened.

Models based on $f(R)$ -gravity that do not require DM halos appear as a viable alternative to generalized NFW models. Due to foreground contamination, we cannot use single frequency maps. For instance, the 217GHz channel could be used to remove the intrinsic CMB component and the signal at other frequencies could be fit to the profile of each individual clusters. Lacking frequency information increases our error bars and makes our final contours wider than what they would be otherwise. Then, the constraints from pressure profiles could be further improve by using frequency information, by carrying out the analysis in foreground clean maps, using the 217GHz map to remove the cosmological CMB signal and fitting the profile of each individual cluster to the data. The conclusion of this and similar studies (Cardone & Capozziello 2011; Napolitano et al. 2012) is that large amounts of DM are not required to describe self-gravitating systems, if we relax the hypothesis that gravity is strictly scale independent above the scale of Solar System.

ACKNOWLEDGMENTS

IDM and FAB acknowledge financial support from the Spanish Ministerio de Educación y Ciencia (grant FIS2012-30926). SC and MDL acknowledge INFN (iniziativa specifica NA12 and OG51).

References

Allemandi, G., et al., 2005, *Gen. Rel. Grav.*, 37, 1891

Model	δ	L (Mpc)	γ	f'_0	f''_0 (kpc $^{-2}$)	χ^2_{dof}
Model A ($L = \zeta < r_{500} >$)	-0.98	1.12	1.07	0.02	-0.003	0.25
Model B	-0.98	1.91	1.07	0.02	-0.001	0.25
Arnaud et al. (2010)	-	-	-	-	-	1.38
Planck Intermediate Results V (2013)	-	-	-	-	-	2.27
Sayers et al. (2013)	-	-	-	-	-	7.70
$\beta(=2/3)$ -model	-	-	-	-	-	15.17

Table 2. χ^2 per degree of freedom (χ^2_{dof}) for the β -model, GFW models with parameters given in Table 1, and for the two $f(R)$ -parametrization considered in this work.

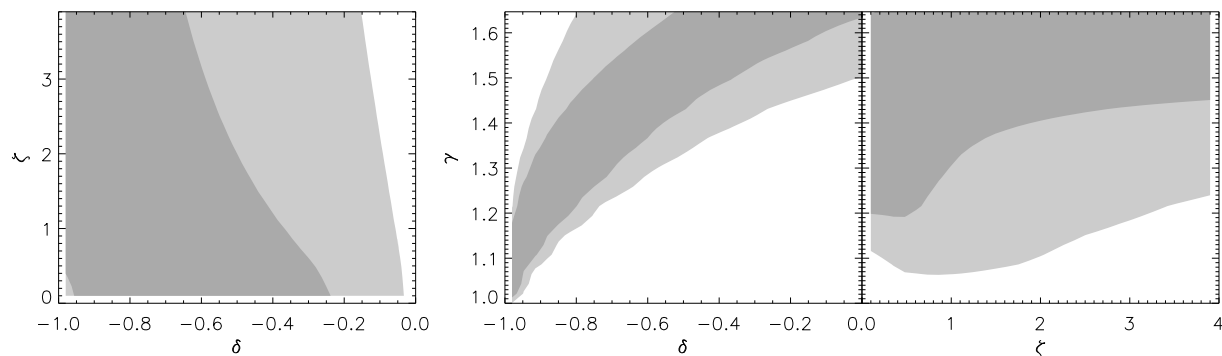


Figure 4. Confidence contours for pairs of parameters of Model A. Contours are at the 68% and 95% confidence level.

Arnaud M., Pratt G. W., Piffaretti R., Böhringer H., Croston, J. H. & Pointecouteau, E., 2010, *A&A*, 517, 92
Arnold, C., Puchwein, E. & Springer, V., 2013, arXiv:1311.5560
Astier, P., et al., 2006, *A&A*, 447, 31
Atrio-Barandela, F., Kashlinsky, A., Kocevski, D. & Ebeling, H., 2008, *ApJ*, 675, L57
Bennett, C.L., et al., 2013, *ApJS*, 208, 20B
Benson, B. A., et al., 2013, *ApJ*, 763, 147
Berry, C. P. L. & Gair, J. L., 2011, *Phys Rev D*, 83, 104022
Blake, C., et al., 2011, *MNRAS*, 418, 1707
Bogdanos C., Capozziello S., De Laurentis M., Nesseris S., 2010, *Astroparticle Physics* 34, 236

Böhringer, H., et al., 2004, *A&A*, 425, 367
Böhringer, H., et al., 2007, *A&A*, 469, 363
Capozziello, S., et al., 2011 *Phys Rev D*, 83, 064004
Capozziello, S., et al., 2012, *Phys Rev D*, 85, 044022
Capozziello, S. & De Laurentis, M., 2011, *Physics Reports*, 509, 167
Capozziello, S. & De Laurentis, M., 2012, *Ann. Phys.*, 524, 1
Capozziello, S., De Filippis, E. & Salzano, V., 2009, *MNRAS*, 394, 947
Capozziello, S. & Troisi, A., 2005, *Phys Rev D*, 72, 044022
Capozziello, S. & Tsujikawa, S., 2008, *Phys Rev D*, 77, 107501

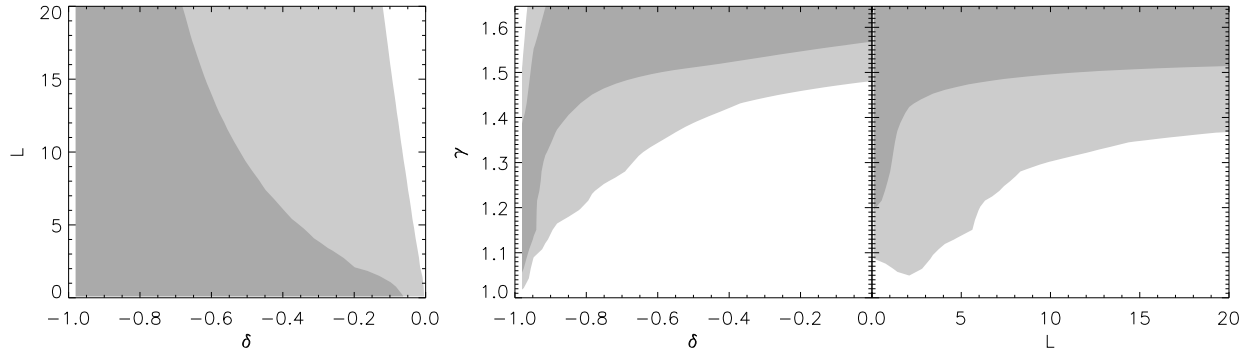


Figure 5. Same as in Fig. 4 for Model B.

- Cardone, V. F. & Capozziello, S., 2011, *MNRAS*, 414, 1301
- Carroll, S.M., Duvvuri, V., Trodden, M. & Turner, M.S., 2004, *Phys Rev D*, 70, 043528
- Cavaliere, A. & Fusco-Femiano, R., 1976, *A&A*, 49, 137
- Cavaliere, A. & Fusco-Femiano, R., 1978, *A&A*, 70, 677
- Clocchiati, A., 2006, *ApJ*, 642, 1
- Clowe, D., et al., *ApJ*, 2006, 648, L109
- De Felice, A. & Tsujikawa, S., 2013, *Living Rev Rel*, 13, 3
- Ebeling, H., Edge, A. C., Allen, S. W., Crawford, C. S., Fabian, A. C. & Huchra, J. P., 2000, *MNRAS*, 318, 333
- Ebeling, H., Edge, A. C., Böhringer, H., Allen, S. W., Crawford, C. S., Fabian, A. C., Voges, W. & Huchra, J. P., 1998, *MNRAS*, 301, 881
- Ebeling, H., Mullis, C. R. & Tully, R. B., 2002, *ApJ*, 580, 774
- Farinelli R., De Laurentis M., Capozziello S., Odintsov S.D., 2013, arXiv: 1311.2744
- Ferraro, S., Schimdtt, F., Hu, W., 2011, *Phys Rev D*, 83, 063503
- Fusco-Femiano, R., Lapi, A. & Cavaliere, A., 2013, *ApJL*, 763, L3
- Gorski, K., et al., 2005, *ApJ*, 622, 759
- Hand, N., et al., 2011, *ApJ*, 736, 39
- Hasselfield, M., et al., 2013, *JCAP*, 07, 008H
- Hinshaw, G., et al., 2013, *ApJS*, 208, 19H
- Hu, W. & Sawicki, I., 2007, *Phys Rev D*, 76, 064004
- Hu, W. & Sawicki, I., 2007, *Phys Rev D*, 76, 104043
- Jones, C., & Forman, W., 1984, *ApJ*, 276, 38
- Kocevski, D. D., Ebeling, H., Mullis, C. R. & Tully, R. B., 2007, *ApJ*, 662, 224
- Komatsu, E., & Seljak, U., 2002, *MNRAS*, 336, 1256
- Komatsu, E., et al., 2011, *ApJS*, 192, 18
- Kravtsov, A. V., & Borgani, S., 2012, *ARAA*, 50, 353
- Lima, N.A. & Liddle, A., 2013, *PhysRevD*, 88, 043521
- Menanteau, F., et al., 2013, *ApJ*, 765, 67
- Nagai, D., Kravtsov, A. V. & Vikhlinin, A., 2007, *ApJ*, 668, 1
- Napolitano, N. R., Capozziello, S., Romanowsky, A. J., Cappacioli, M. & Tortora, C., 2012, *ApJ*, 748, 87
- Navarro, J. F., Frenk, C. S., White, S. D. M., 1997, *ApJ*, 490, 493
- Nojiri S. and Odintsov S. D., 2007, *Geom. Meth. Mod. Phys.*, 4, 115
- Nojiri S. and Odintsov S. D., 2011, *Phys. Rept.*, 505, 59
- Piffaretti, R., et al., 2011, *A&A*, 534, A109
- Plagge, T., et al., 2010, *ApJ*, 716, 1118
- Planck Collaboration. Planck Early Results X: Statistical analysis of Sunyaev-Zeldovich scaling relations for X-ray galaxy clusters, 2011, *A&A*, 536, A10
- Planck Collaboration. Planck Intermediate Results V: Pressure profiles of galaxy clusters from the Sunyaev-Zeldovich effect, 2013, *A&A*, 550, 131
- Planck Collaboration. Planck Intermediate Results X: Physics of the hot gas in the Coma cluster, 2013, *A&A*,

554, 140

Planck Collaboration. Planck 2013 results I: Overview of products and scientific results, 2013, A&A, submitted. arXiv:1303.5062

Planck Collaboration. Planck 2013 results XII: Component separation, 2013, A&A, submitted. arXiv:1303.5072

Planck Collaboration. Planck 2013 results. XIII: Galactic CO emission, 2013, A&A, submitted. arXiv:1303.5073

Planck Collaboration. Planck 2013 results XV: CMB power spectra and likelihood, 2013, A&A, submitted. arXiv:1303.5075

Planck Collaboration. Planck 2013 results. XVI: Cosmological parameters, 2013, A&A, submitted. arXiv:1303.5076

Planck Collaboration. Planck 2013 results XX: Cosmology from Sunyaev-Zeldovich cluster counts, 2013, A&A, submitted. arXiv:1303.5080

Planck Collaboration. Planck 2013 results XXI: Cosmology with the all-sky Planck Compton parameter y -map, 2013, A&A, submitted. arXiv:1303.5081

Planck Collaboration. Planck 2013 results XXIX: Planck catalogue of Sunyaev-Zeldovich sources, 2013, A&A, submitted. arXiv:1303.5089

Quandt, I. & Schmidt, H. J., 1991, *Astron. Nachr.*, 312, 97

Riess, A. G., et al., 2004, *ApJ*, 607, 655

Sanders, R. H., 1984, *A&A*, 136, L21

Sawicki, I. & Hu, W., 2007, *Phys Rev D*, 75, 127502

Sayers, J., et al., 2013, *ApJ*, 768, 177

Schimdt, F., Vikhlinin A. & Hu, W., 2009, *Phys. Rev. D*, 80, 083505

Sehgal, N., et al., 2011, *ApJ*, 732, 44

Song, Y.-S., Hu, W. & Sawicki, I., 2007, *Phys Rev D*, 75, 044004

Sotiriou, T.P. & Faroni, V., 2010, *Rev Mod Phys*, 82, 451

Staniszewski, Z., et al., 2009, *ApJ*, 701, 32

Sunyaev, R. A. & Zeldovich, Y. B., 1972, *Comments on Astrophys. Space Phys.*, 4, 173

Sunyaev, R. A. & Zeldovich, Y. B., 1980, *MNRAS*, 190, 413

Suto, Y., Sasaki, S. & Makino, N., 1998, *ApJ*, 509, 544

White, D. A., Jones, C. & Forman, W., 1997, *MNRAS*, 292, 419

Williamson, R., et al., 2011, *ApJ*, 738, 139

Vanderlinde, K., et al., 2010, *ApJ*, 722, 1180